Naringin Effect on SARS-CoV-2 Pseudovirus Entry and Spike Mediated Syncytia Formation in hACE2-overexpressing Cells

Endah Puji Septisetyani[1*], Pekik Wiji Prasetyaningrum[1], Komang Alit Paramitasari[1], Ahmad Suyoko[1], Alayna Lillahida Indri Himawan[1], Salsabila Azzahra[1,2], Popi Hadi Wisnuwardhani[1], Khairul Anam[3], Ratna Dwi Ramadani[1,4], Adi Santoso[1], Ratih Asmana Ningrum[1], Neng Herawati[1], Yana Rubiyana[1]

[1]Research Center for Genetic Engineering, National Research and Innovation Agency (BRIN), KST Soekarno, Cibinong, Bogor 16911, Indonesia
[2]Department of Biology, Faculty of Mathematic and Life Sciences, Republic of Indonesia Defense University, Indonesia Peace and Security Center (IPSC), Sentul, Bogor, Indonesia
[3]Research Center for Applied Microbiology, National Research and Innovation Agency (BRIN), KST Soekarno, Cibinong, Bogor 16911, Indonesia
[4]PT Etana Biotechnologies Indonesia, Kw. Industri Pulo Gadung, Jatinegara, Jakarta 13930, Indonesia

ARTICLE INFO

ABSTRACT

A molecular docking study demonstrates the interaction between naringin, a citrus flavonoid, with SARS-CoV-2 spike RBD. Nevertheless, *in vitro* investigation of the inhibitory effect of naringin on SARS-CoV-2 entry and syncytia models has yet to be carried out. We synthesized VSVΔG-GFP/Spike* pseudovirus (PSV) as a SARS-CoV-2 model by pseudotyping VSVΔG-GFP/S* in BHK-21 cells overexpressing the SARS-CoV-2 spike glycoprotein. In the SARS-CoV-2 PSV entry assay, we utilized CHO-K1 cells transfected with hACE2 plasmid, which were then treated with naringin and SARS-CoV-2 PSV/naringin. After 16-18 h incubation, PSV internalization represented by the GFP signal was observed under a fluorescence microscope. Immunofluorescence staining was also performed to probe the SARS-CoV-2 spike and confirm the PSV entry. We performed a syncytia assay using 293T cells co-transfected with SARS-CoV-2 spike/hACE2. Six hours after transfection, the cells were treated with naringin and incubated for another 16-18 hours. Then, we observed syncytia using a phase contrast microscope. Based on fluorescence foci quantification, the results indicated that naringin might inhibit SARS-CoV-2 PSV entry at a concentration of 100 μM (P<0.05). However, naringin did not prevent syncytia formation compared to solvent control. These PSV entry and syncytia assay results suggested that naringin potentially inhibited SARS-CoV-2 viral infection but not cell-to-cell viral transmission.

1. Introduction

SARS-CoV-2 is a highly pathogenic virus that causes the worldwide COVID-19 pandemic (Hu 2020). This virulent coronavirus contains spike S glycoprotein on its surface containing S1 and S2 sub-units (Noman *et al.* 2021). This S1 sub-unit bears a receptor binding domain (RBD) that is responsible for binding its target receptor, human angiotensin-converting enzyme-2 (hACE2), and mediating cellular entry (Huang *et al.* 2020). Meanwhile, TMPRSS2, a transmembrane protease, facilitates cell surface entry by membrane fusion (Hoffmann *et al.* 2020) (Jackson *et al.* 2022). Therefore, for screening SARS-CoV-2 cell entry inhibitors, *in silico* molecular docking has been widely applied by targeting either RBD or the receptors hACE2 and TMPRSS2 (Yan *et al.* 2022). Moreover, for targeting the replication process, *in silico* studies have been performed on SARS-CoV-2 protease 3CLpro and PLpro (Narayanan *et al.* 2022).

Naringin is a flavanone-7-O-glycoside mainly found in the orange (*Citrus reticulata*) peel (Sharma *et al.* 2019). It shows several bioactivities, including anti-inflammatory, antioxidant, and chemoprevention

* Corresponding Author
  E-mail Address: enda041@brin.go.id

(Yi *et al.* 2017). Recently, a molecular docking study showed the interaction of naringin with structural and non-structural proteins of SARS-CoV-2, which involve Spike RBD, 3CLpro, and PLpro. Naringin binds SARS-CoV-2 RBD at SER 494 and GLN 493 (Bhowmik *et al.* 2021).

Glycosylated flavonoids generally show higher bioavailability than aglycone (Xiao 2017). In addition, glycosylated flavonoids often show higher binding affinity to their receptors than aglycone (Xiao *et al.* 2009). In line with this data, naringin also shows higher binding affinity toward TMPRSS2, SARS-CoV-2 3CLpro, and PLpro than its aglycone, naringenin. The glycosyl group has been reported to be responsible for decreasing the binding energy toward those receptors (Kumar *et al.* 2022). Unlike naringin, naringenin as anti-SARS-CoV-2 has been studied in Vero cells (Clementi *et al.* 2021). The Vero cells are cultured and treated with naringenin and SARS-CoV-2 at MOI 0.01. In this research, Clementi *et al.* (2021) reported that naringenin inhibits the SARS-CoV-2-induced cytopathic effect (CPE) of Vero cells in a concentration-dependent manner. Moreover, despite the potential impact of naringenin, the in vitro effect of naringin on SARS-CoV-2 infection has yet to be performed.

SARS-CoV-2 can infect the target cells by direct infection or via cell-to-cell transmission. Hence, our study aimed to investigate the effect of naringin on SARS-CoV-2 entry utilizing the pseudovirus (PSV) platform on CHO-K1 cells overexpressing hACE2. The study of entry inhibitors using live SARS-CoV-2 virus needs a BSL3 containment, limiting the number of laboratories to perform the assay. PSV, a chimeric virus that can be engineered to be non-replicative, plays an essential role in providing a surrogate assay that is relevant to the original virus. SARS-CoV-2 PSV enables the screening of cell entry inhibitors in BSL2 laboratories (Septisetyani *et al.* 2021). We also investigated the inhibitory effect of naringin on cell-to-cell transmission by using syncytia models.

2. Materials and Methods

2.1. Cell Culture and Reagents

BHK-21/WI-2 cells (Kerafast EH1011, USA) used for pseudotyping were cultured in DMEM medium (Sigma, USA) supplemented with 5% FBS (Sigma, USA), 100 I.U./ml Penicillin and 100 μg/ml Streptomycin (Sigma, USA). In addition, CHO-K1 cells (ECACC 85051005, UK) were maintained in an F12 medium (Sigma, USA) supplemented with 10% FBS. Plasmid pCAGGS-G-Kan (EH1017) and pseudotyped rVSVΔG-GFP (EH1019-PM) were obtained from Kerafast (USA), while pcDNA3.1-SARS2-Spike (a gift from Fang Li; Addgene plasmid #145032), (Shang *et al.* 2020), pcDNA3.1-hACE2 (a gift from Fang Li; Addgene plasmid #145033) (Shang *et al.* 2020),, and pCDNA_Lifeact-GFP_NLS-mCherry (a gift from Olivier Pertz; Addgene plasmid # 69058) were obtained from Addgene (USA). Plasmid transfection was performed by using Lipofectamin-Ltx (Invitrogen, USA) or polyethyleneimine ((PEI MAX®-Transfection Grade Linear Polyethylenimine Hydrochloride (MW 40,000), Polysciences, USA). Flavonoid naringin was obtained from Sigma (USA).

2.2. Synthesis of SARS-CoV-2 PSV

For pseudotyped rVSV amplification, about 80% of the confluence monolayer of BHK-21 cells were transfected with pCAGGS-G-Kan using lipofectamine-Ltx with 1:3 of DNA to PEI ratio. The following day, syncytia were observed due to the expression of G glycoprotein. Next, the culture medium was replaced with a three ml medium containing pseudotyped rVSVΔG-GFP at MOI 0.1 and incubated for one hour in a CO_2 incubator. At the end of incubation, 7 ml of fresh culture medium was added, and incubation was continued overnight. Pseudotyped rVSV was collected from the conditioned medium after observation of cytopathic effects. BHK-21 cells were transfected with pcDNA3.1-SARS2-Spike plasmid using a similar transfection protocol to express SARS-CoV-2 spike glycoprotein to generate SARS-CoV-2 PSV. The next day, the culture medium was replaced with a three ml medium containing pseudotyped rVSV-ΔG-GFP at MOI ~3 and incubated for one hour in a CO_2 incubator. Then, the medium was aspirated, and the cells were washed with PBS once. A ten-milliliter medium containing 1:2,000 anti-VSV-G antibodies was added to the cells and then incubated overnight. Condition medium was collected the following day after the cytopathic effect was observed to obtain PSV. Cell debris was separated by centrifugation at 1320 G for 10 min, and the supernatant was aliquoted and stored at -80°C deep freezer.

2.3. Western Blot

Cells after transfection were collected as cell pellets and stored at -20°C. The cells were then lysed using ice-cold RIPA buffer (Abcam, USA) with the addition of a protease inhibitor cocktail and incubated for 15-20 min on ice. The lysate was then spun to remove cell debris. The total protein concentration of cell lysates was determined by BCA assay (Thermo Scientific) using BSA (Sigma, USA) as standard. For SDS-PAGE, about 10-40 µg protein was resolved in a 10% denatured polyacrylamide gel and transferred onto an activated PVDF membrane. Then, the membrane was incubated in blocking buffer (5% skim milk in TBS/0.05% tween-20) followed by blotting with primary antibodies (1:2,000 rabbit anti-SARS-CoV-2 spike antibody (ab275759, Abcam, USA); 1:2,000 rabbit anti-VSV-G antibody (PA1-30138, Invitrogen, California, USA), or 1:4,000 mouse anti-β-actin antibody (A2228, Sigma, USA)) for two hours at room temperature or overnight at 4°C. After washing with TBS/T, the membrane was incubated in secondary antibodies (1:4,000 HRP conjugated antibodies (goat anti-rabbit IgG H&L ab205718, Abcam, USA and rabbit anti-mouse IgG H&L ab6728, Abcam, USA), or 1:10,000 IR-Dye conjugated antibodies (IRDye-680 RD, LI-COR, USA)) in blocking buffer for about two hours at room temperature. Western blot signal was detected by incubating the membrane with chemiluminescence substrate (LI-COR) and exposed in a film (Fuji film) developed with a developer kit (Ilford) or observed by using a LI-COR Odyssey CLx.

2.4. MTT Cell Viability Assay

CHO-K1 cells were seeded 70,000 cells/ml onto a 96-well plate. The next day, freshly prepared serial dilution of naringin at concentrations of 1, 10, 25, 50, 75, 100, 200, and 500 µM was added each 100 µl per well in quadruplet. The cells were then incubated for 20 h before MTT (Gibco, USA) treatment. MTT was added to each well with a final concentration of 0.5 mg/ml. After two h incubation, the MTT solution was removed, and the formazan formed within the viable cells was dissolved using DMSO (AppliChem, Germany), and the optical density of each well was determined at λ = 570 nm. Relative cell viability was quantified using the formula = (OD treatment : OD control) × 100%.

2.5. Immunofluorescence Staining

Cells grown on a coverslip were fixed with 4% paraformaldehyde (Elabscience, USA). After blocking with 1% BSA, the cells were incubated with primary antibody (rabbit anti-hACE2 antibody (SAB3500971, Sigma, USA) or mouse anti-spike S1 sub-unit antibody (MAB105403, R&D system, USA)) at a 1:250 ratio, followed with fluorochrome-conjugated secondary antibodies (goat anti-rabbit IgG H&L (Alexa Fluor® 488) ab150077, Abcam, USA and Goat Anti-Rabbit IgG H&L (Alexa Fluor® 594) ab150080, Abcam, USA) at a 1:1,000 ratio. The cells were then mounted with a DAPI mountant (Abcam, USA). The fluorescence signal was observed using a motorized fluorescence microscope (Olympus IX83, Japan).

2.6. PSV Entry Assay

PSV entry assay was performed in CHO-K1 cells overexpressing hACE2. Briefly, an 8-well chamber slide (SPL Life Science, Korea) was coated with poly-D-lysine (Gibco, USA), and CHO-K1 cells were seeded at a density of 40,000 cells/well. After overnight incubation, the cells were transfected with a plasmid encoding hACE2 by PEI transfection. The following day, the medium was refreshed, and the cells were preincubated with naringin for 30 min. Then, the medium was replenished with a new medium containing PSV with a titer 1:2 (Supplementary Figure 1) and a similar concentration of naringin and incubated overnight. At the end of incubation, the cells were fixed and stained for SARS-CoV-2 spike. The image was acquired using a motorized fluorescence microscope (Olympus IX-83). Using Fiji software, PSV entry was determined by counting the GFP fluorescence foci representing internalized PSV particles. The data were presented as the number of fluorescence foci per field or infected cells (%).

2.7. Syncytia Formation Assay

Several 160,000 cells/ml of 293T cells were seeded onto a 24-well plate and incubated overnight. The next day, the cells were transfected with plasmids encoding SARS-CoV-2 Spike, hACE2, and lifeact-GFP/NLS-mCherry using PEI with a DNA to PEI ratio of 1:3. Six hours after transfection, the transfection mix was removed and replaced with 100 µM naringin in culture medium or 2% DMSO as solvent control. After 16-18 h incubation, syncytia formation was

investigated using an inverted phase contrast microscope. In addition, to confirm the syncytia formation, lifeact-GFP expression was observed under a fluorescence microscope (Olympus-IX83) to investigate the formation of multinucleated giant cells.

2.8. Statistical Analysis

The significant difference of each treatment was analyzed by t-test using Microsoft Excel (Microsoft, USA).

3. Results

3.1. Synthesis of SARS-CoV-2 PSV

We successfully synthesized the SARS-CoV-2 PSV-bearing VSV backbone with a GFP reporter. This non-replicative PSV was generated using a recombinant VSV lacking a gene that encodes G glycoprotein (rVSVΔG-GFP). For rVSV synthesis and amplification, the G glycoprotein gene was complemented by adding the plasmid bearing the G glycoprotein gene (Figure 1A). By using this method, VSV will not generate new competent viruses after cellular internalization. The same procedure was applied for SARS-CoV-2 pseudotyping. The SARS-CoV-2 PSV was generated by incorporating spike S glycoprotein (Spike) into pseudotyped rVSVΔG-GFP (rVSVΔG-GFP/G*) (Figure 1B). To eliminate the excessive amount of rVSVΔG-GFP/G* that will give redundant data, the medium containing rVSVΔG-

redundant data, the medium containing rVSVΔG-GFP /G* was removed after one-hour incubation, cells were washed with PBS, and anti-VSV-G antibody was added to neutralized rVSVΔG-GFP/G*. During rVSVΔG-GFP /G* amplification and SARS-CoV-2 pseudotyping, we observed GFP fluorescence that indicated rVSVΔG-GFP /G* internalization and viral protein expression (Figure 1C and D). Even though during VSV and SARS-CoV-2 pseudotyping, the rVSVΔG-GFP /G* was added at different amounts (0.1 vs ~3 MOI), the GFP signal was observed to be stronger in BHK-21 cells during VSV pseudotyping. This data indicated that new rVSVΔG-GFP /G* secreted during VSV pseudotyping could re-infect the cells and produce more PSV. Whereas rVSVΔG-GFP /S* could not infect BHK-21 cells; thus, the PSV titer was lower at the end of the pseudotyping process (Figure 2). This data also indicated the formation of rVSVΔG-GFP/S* in which the excessive amount of rVSVΔG-GFP/G* was unlikely to occur.

Furthermore, we conducted a Western blot of cell lysates to confirm the expression of VSV-G and spike. We also performed a Western blot for the conditioned medium collected after pseudotyping to ensure the integration of the SARS-CoV-2 spike into the rVSVΔG-GFP backbone and the formation of PSV (Figure 2). The results indicated that BHK-21 cells transfected with pCAGGS-G-Kan or pCDNA3.1-SARS2-Spike expressed VSV-G or SARS-CoV-2 spike glycoprotein. Moreover, VSV-G was observed in the conditioned medium after VSV pseudotyping but
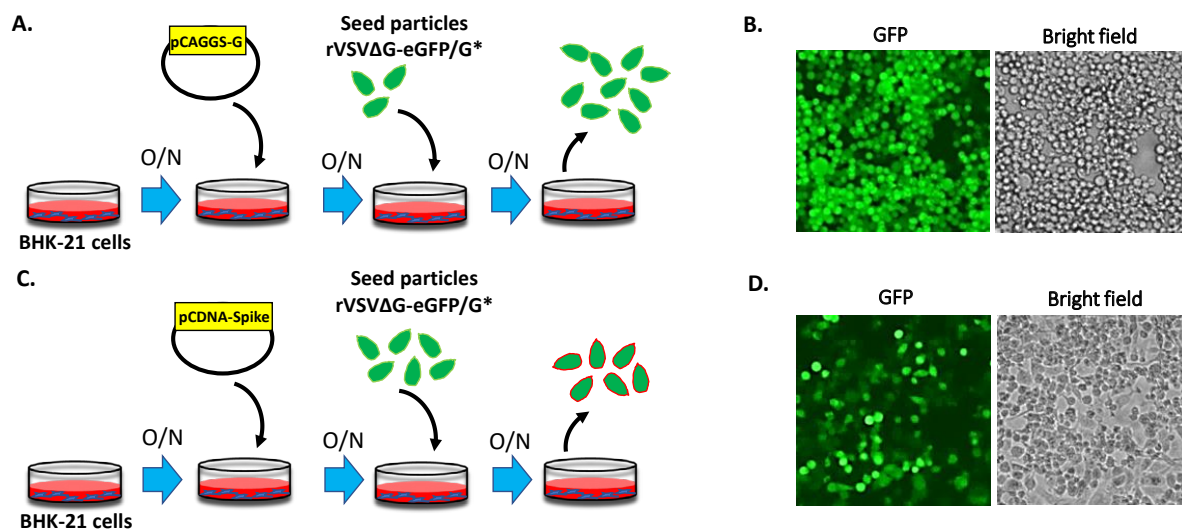

Figure 1. Synthesis of SARS-CoV-2 pseudovirus in BHK-21 cells. (A-B) Schematic representation of VSV amplification and the observation of GFP expression and cytopathic effect. (C-D) Schematic representation rVSVΔG-eGFP/S* pseudotyping and the observation of GFP expression and cytopathic effect
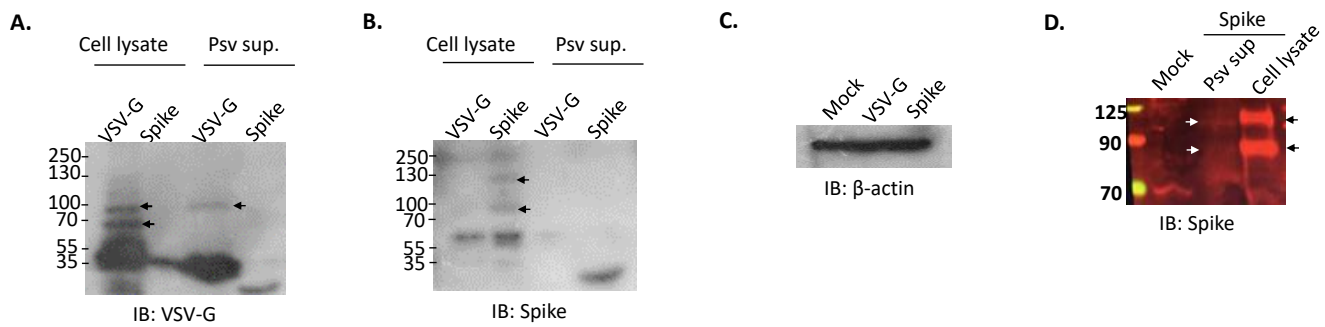
Figure 2. Western blot analysis of BHK-21 cell lysates and supernatants. Detection of VSV-G (A), SARS-CoV-2 spike (B), and β-actin (C) by chemiluminescence and SARS-CoV-2 spike (D) by far IR-fluorescence

not in the conditioned medium after SARS-CoV-2 pseudotyping. The spike signal in the conditioned medium was lower than that of the VSV-G signal. This data represented less rVSVΔG-GFP/S* produced during SARS-CoV-2 pseudotyping than the number of rVSVΔG-GFP/G* formed during VSV pseudotyping.

3.2. Confirmation of hACE2 Expression in CHO-K1 Cells and PSV Internalization

To analyze the functionality of hACE2-encoding plasmid, we observed the expression check in CHO-K1 cells. ACE2 expression and cellular localization were observed by immunofluorescence staining. ACE2 was detected and localized in the cell membrane as a transmembrane receptor, as we did not permeabilize the cells during the immunostaining process. Moreover, cell lysate after hACE2 transfection was prepared in RIPA buffer for Western blot. The results indicated hACE2 expression detected by anti-ACE2 antibody, while non-transfected cells as control cells did not show detectable protein bands in a similar size (Figure 3).

Next, we clarified SARS-CoV-2 entry in hACE2 expressing CHO-K1 cells. The cells were transfected with a plasmid encoding hACE2 one day before PSV treatment. On the treatment day, the cells were treated with SARS-CoV-2 PSV and incubated for about 18 hours in a CO_2 incubator. PSV internalization was observed by fluorescence microscope to investigate GFP expression. In addition, to detect the presence of Spike protein, we used an anti-spike antibody and blotted it with a secondary antibody conjugated with Alexa-594. Thus, the Spike signal appeared red. The results showed that GFP fluorescence foci were detected in hACE-expressing CHO-K1 cells and colocalized with cells with Spike signal resulting from antibody reaction (Figure 4). In addition, the GFP
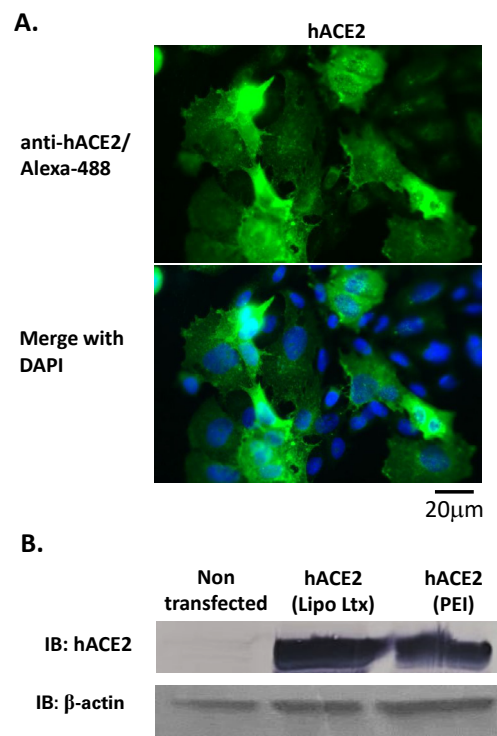

Figure 3. Analysis of hACE2 expression in CHO-K1 cells. (A) Representative image of immunofluorescence staining of hACE2, (B) western blot analysis from cell lysates after exogenous hACE2 expression

expression was observed 5 hours after the addition of PSV in the CHO-K1 cells expressing hACE2. Whereas a similar phenomenon did not appear in the control CHO-K1 cells. This data indicates the selectivity of the PSV entry process (Supplementary Figure 2).

3.3. Cytotoxicity Assay of Naringin in CHO-K1 Cells

To confirm that the naringin concentration used for treatment did not cause significant harmful effects on cells, we carried out cell viability studies. Based on

the MTT assay, naringin concentrations of 1, 10, 25, 50, 75, 100, 200, and 500 µM did not significantly affect the cell viability (Figure 5). Thus, naringin showed no cytotoxic effects on CHO-K1 cells, representing normal cells.
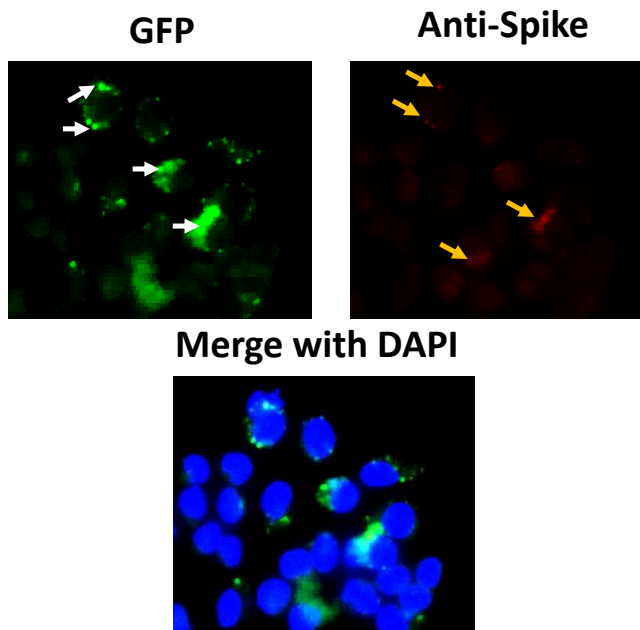
GFP | Anti-Spike

Merge with DAPI

Figure 4. Pseudovirus internalization in hACE2 expressing CHO-K1 cells. Representative image of pseudovirus entry after overnight incubation indicated colocalization of GFP fluorescence foci with Spike signals from antibody reaction. White arrow indicates GFP foci, while orange arrow indicates Spike signals
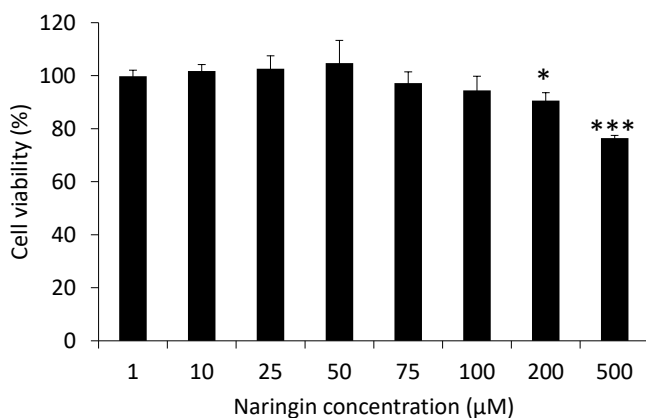

Figure 5. Cell viability assay of naringin in CHO-K1 cells. Cells were seeded at a density of 7,000 cells/well of 96-well plate. The Naringin concentration used for treatment was as indicated in the graph. The cells were incubated for about 20 h with naringin before MTT treatment. n = 4 for each treatment

3.4. Inhibition of PSV Entry by Naringin

After confirmation of SARS-CoV-2 PSV entry in hACE2-expressing CHO-K1 cells, we examined the effect of naringin on SARS-CoV-2 PSV entry by utilizing hACE2-transfected CHO-K1 cells. Here, we investigated the internalization of the SARS-CoV-2 PSV by observing the GFP fluorescence foci that represented the surrogate SARS-CoV-2 infection (Figure 6A). Then, we quantified the GFP foci of five to six digital microscope images for each treatment using the image analysis software FIJI. The results showed that the average number of fluorescence foci per area in 10 µM naringin-treated cells (67) was not statistically different from the number of fluorescence foci in DMSO control (137.17). Furthermore, treatment with naringin 100 µM (124.83) could significantly decrease the number of PSV particles compared to solvent control (222) ($P<0.05$) (Figure 6B). However, when we analyzed the percentage of infected cells, there were no significant differences between naringin-treated and control cells. These results might indicate that naringin could inhibit PSV infection rate for each cell but not statistically reduce the total number of infected cells (Figure 6C).

3.5. Syncytia Formation Assay in Spike/hACE2 Expressing Cells

Syncytia can be formed due to Spike interaction with its receptor, hACE2. In this experiment, we co-expressed Spike, hACE2, and lifeact-GFP/NLS-mCherry in 293T cells. Spike expressed in one cell will localize in the cell membrane and be capable of binding hACE2 of the adjacent cells. The two cells generally will fuse and form multinucleated cells. In addition, using a fluorescence microscope, lifeact-GFP/NLS-mCherry expression helped locate and confirm the syncytia. Lifeact-GFP locates the cytoplasmic actin, while NLS-mCherry locates the nucleus area. As a result, we observed syncytia with multinuclei and grouped them based on the nuclei number.

The syncytia could be observed using a phase contrast microscope (Figure 7A). Moreover, we also investigated the syncytia using a fluorescence microscope to confirm the expression of lifeact-GFP/NLS-mCherry expression as a fluorescence biomarker (Figure 7B). However, the results indicated that naringin did not significantly affect syncytia formation in the transfected cells (Figure 7C).
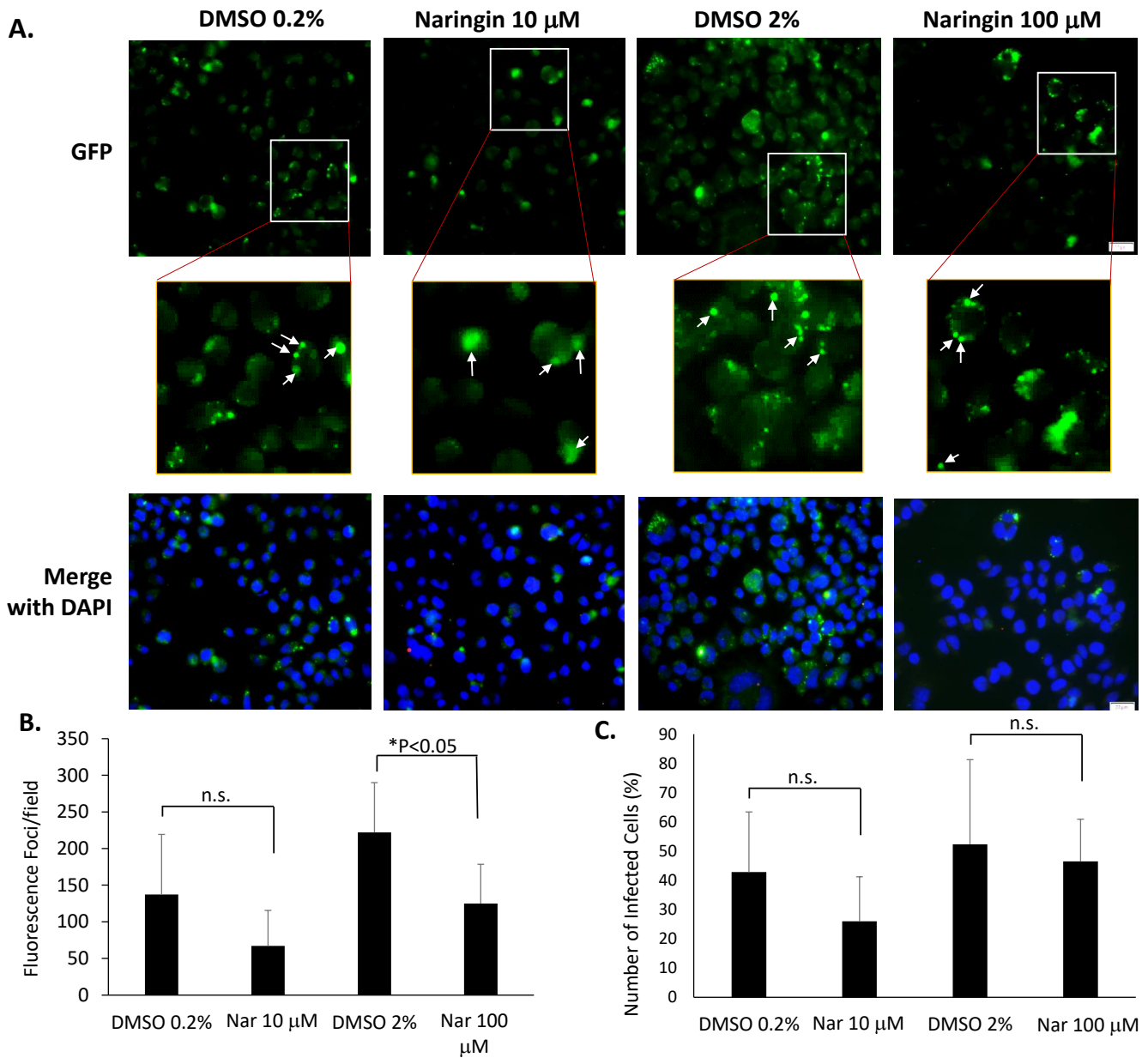
A.

B.

C.

Figure 6. Effect of naringin on SARS-CoV-2 PSV entry. (A) Representative images showing GFP foci in naringin treated cells and control cells, (B) quantification of fluorescence foci per field, (C) quantification percentage of infected cells. * = statistical significance, P<0.05. Bar = 20 μm. White arrow shows representative fluorescence foci counted in PSV entry assay. n = 5-6 images for each treatment that acquired using a motorized fluorescence microscope
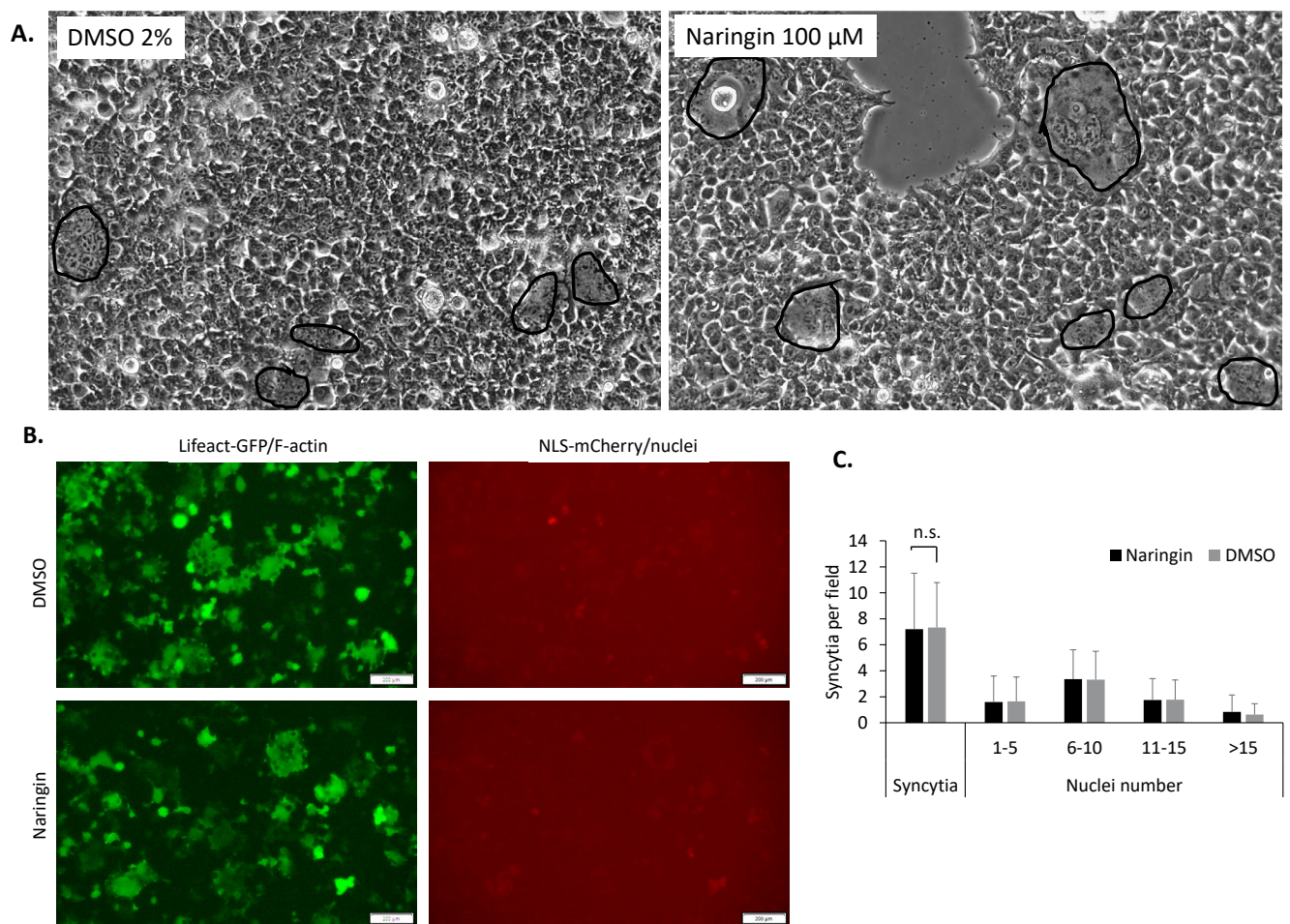
Figure 7. Effect of naringin on syncytia formation. (A–B) Representative images of syncytia formed in 293T/Spike/hACE/ Lifeact-GFP/NLS-mCherry after treated with naringin or DMSO, (C) quantification of syncytia on the treated cells. Black curve line indicates syncytia. n=49 and 67 images from 2 independent experiments

4. Discussion

SARS-CoV-2 is a highly virulent and pathogenic virus with a global fatality rate of about 1%. The virus has evolved and generated new variants that can re-infect the same individuals (Lamers and Haagmans 2022) (Mahajan *et al.* 2021). WHO classifies this virus into virus risk group 3. Therefore, virus propagation research must be conducted within a BSL3 laboratory (Kaufer *et al.* 2020). Consequently, several SARS-CoV-2 antiviral research studies have been conducted *in silico* using molecular docking software because of the limited number of BSL3 facilities. In line with these facts, PSV has provided an alternative for studying antiviral compounds, especially at the cell entry stage (Hu *et al.* 2020). By synthesizing a chimeric virus using a risk group 2 viral backbone integrated with SARS-CoV-2 spike glycoprotein, we can perform an entry inhibitor assay in a BSL2 laboratory (Sun *et*

al. 2022). In this study, we synthesized SARS-CoV-2 PSV utilizing pseudotyped rVSVΔG-GFP developed by Whitt (2010). The SARS-CoV-2 pseudotyping procedure was done in BHK-21 cells expressing the SARS-CoV-2 spike. BHK-21 cells were chosen for pseudotyping using the VSV backbone because VSV-G-mediated infection occurs more effectively in animal cells. It was shown that although BHK-21 cells were infected with a lower MOI for VSV amplification than during SARS-CoV-2 pseudotyping, GFP fluorescence appeared higher (Figure 1). However, a problem arose with a remaining pseudotyped rVSV-ΔG-GFP in the conditioned medium collected after SARS-CoV-2 pseudotyping, which would be used for the cell entry inhibitor assay. As a solution, the anti-VSV-G antibody was added to the cells during the pseudotyping process, as was done by Almahboub *et al.* (2020).

As it is known that the SARS-CoV-2 virus enters the cells through the interaction between the spike and hACE2, cells that do not express hACE2 have low viral tropism or do not have a tropism for SARS-CoV-2 (Liu *et al.* 2021) (Murgolo *et al.* 2021). However, some cells, such as Vero cells, can uptake viruses with non-specific mechanisms (Kiesslich and Kamen 2020). Therefore, we used hACE2-expressing CHO-K1 cells to avoid unspecified entry. We demonstrated that the synthesized PSV entered into CHO-K1 cells transfected with hACE2 and found that GFP foci were colocalized with Spike signal from the antibody reaction. These data implied that the GFP foci represented Spike PSV (Figure 4).

Furthermore, as we used GFP as a reporter in this PSV system, the VSV genome contained a GFP genetic material that will be expressed once the pseudovirus is internalized into the cells. Therefore, the longer incubation time following PSV treatment will result in the more accumulated GFP within the cells as well as the brighter GFP signal. In contrast, the spike as the outer protein of SARS-CoV-2 is incorporated into the surface of the VSV backbone and there is no RNA expressing SARS-CoV-2 spike in the VSV genome. Therefore, no new spike protein expression will follow the pseudovirus entry. The spike detected from this experiment originated from the remaining pseudovirus particle itself.

Naringin is a potential compound candidate as an entry inhibitor for SARS-CoV-2 based on the *in silico* test (Kiesslich and Kamen 2020) (Magiorkinis 2022). Even so, no experimental tests have been conducted in the laboratory that show entry inhibitory activity in the SARS-CoV-2 virus or PSV models. In this study, we demonstrated the effect of naringin on SARS-CoV-2 PSV entry. Our results show that naringin can potentially inhibit PSV entry in CHO-K1 cells transfected with the plasmid encoding hACE2. This is shown in the decreased GFP signal observed after treatment with naringin compared to DMSO as solvent control, especially at a concentration of 100 µM (Figure 6). We observed GFP expression as green fluorescence foci appeared within the cells and counted for each focus. As the SARS-CoV-2 nucleocapsid N protein is detected and localizes within the stress granules of infected cells, the GFP foci we found here were similar to those images reported by Savastano *et al.* (2020). The GFP focus might present more than one focus per cell, which might indicate multiple PSV infections.

Syncytia is reported to be found in severe cases of COVID-19 (Lin *et al.* 2021). The interaction between the spike and its target receptor has been known to underlay syncytia formation, mediating cell-to-cell infection of SARS-CoV-2 (Buchrieser *et al.* 2020). In our experiments, naringin did not significantly inhibit SARS-CoV-2 cellular transmission. However, as reported for naringenin (Clementi *et al.* 2021), naringin may also work on the same intracellular target to inhibit SARS-CoV-2 replication.

Furthermore, to confirm these results, the entry test can be performed on CHO-K1 cells that express two proteins, hACE2 and TMPRSS2, or model cells that have good tropism for SARS-CoV-2 such as Calu3 cells, lung epithelial cells, which express hACE2 as well as TMPRSS2 so that these cells can mediate the entry of SARS-CoV-2 through the cell surface entry/cell fusion mechanism. In addition, the affinity between naringin and PSV can be studied using surface plasmon resonance on samples containing soluble hACE2.

To conclude, according to the SARS-CoV-2 PSV cell entry inhibitor assay, our results revealed that naringin decreased SARS-CoV-2 PSV entry compared to DMSO as solvent control at a concentration of 100 µM (P<0.05). Moreover, the PSV entry and syncytia assay results suggested that naringin potentially inhibited SARS-CoV-2 viral infection but not cell-to-cell viral transmission.

Acknowledgements

References

Almahboub, S.A., Algaissi, A., Alfaleh, M.A., ElAssouli, M.Z., Hashem, A.M. 2020. Evaluation of neutralizing antibodies against highly pathogenic coronaviruses: a detailed protocol for a rapid evaluation of neutralizing antibodies using vesicular stomatitis virus pseudovirus-based assay. *Front. Microbiol.* 11, 2020. https://doi.org/10.3389/fmicb.2020.02020

Bhowmik, D., Nandi, R., Prakash, A., Kumar, D. 2021. Evaluation of flavonoids as 2019-nCoV cell entry inhibitor through molecular docking and pharmacological analysis. *Heliyon.* 7, p.e06515.https://doi.org/10.1016/j.heliyon.2021.e06515

Buchrieser, J., Dufloo, J,, Hubert, M., Monel, B., Planas, D., Rajah, M.M., Planchais, C., Porrot, F., Guivel-Benhassine, F., Van der Werf, S., Casartelli, N., Mouquet, H., Bruel, T., Schwartz, O. 2020. Syncytia formation by SARS-CoV-2-infected cells. *EMBO J.* 39, e106267. https://doi.org/10.15252/embj.2020106267

Clementi. N., Scagnolari, C., D'Amore, A., Palombi, F., Criscuolo, E., Frasca, F., Pierangeli, A., Mancini, N., Antonelli, G., Clementi, M., Carpaneto, A., 2021. Naringenin is a powerful inhibitor of SARS-CoV-2 infection *in vitro. Pharmacol. Res.* 163, p.105255. https://doi.org/10.1016/j.phrs.2020.105255

Hoffmann, M., Kleine-weber, H., Schroeder, S., Krüger, N., Herrler, T., Erichsen, S., Schiergens, T.S., Herrler, G., Wu, N.H., Nitsche, A., Müller, M.A., Drosten, C., Pöhlmann, S. 2020. SARS-CoV-2 cell entry depends on ACE2 and TMPRSS2 and is blocked by a clinically proven protease inhibitor. *Cell.* 181, 271-280. https://doi.org/10.1016/j.cell.2020.02.052

Hu, J., Gao, Q., He, C., Huang, A., Tang, N., Wang, K. 2020. Development of cell-based pseudovirus entry assay to identify potential viral entry inhibitors and neutralizing antibodies against SARS-CoV-2. *Genes Dis.* 7, 551-557. https://doi.org/10.1016/j.gendis.2020.07.006

Huang, Y., Yang, C., Xu, X.F., Xu, W., Liu, S.W. 2020. Structural and functional properties of SARS-CoV-2 spike protein: potential antivirus drug development for COVID-19. *Acta Pharmacol. Sin.* 41, 1141-1149. https://doi.org/10.1038/s41401-020-0485-4

Jackson, C.B., Farzan, M., Chen, B., Choe, H., 2022. Mechanisms of SARS-CoV-2 entry into cells. *Nat. Rev. Mol. Cell. Biol.* 23, 3-20. https://doi.org/10.1038/s41580-021-00418-x

Kaufer, A.M., Theis, T., Lau, K.A., Gray, J.L, Rawlinson, W.D. 2020. Laboratory biosafety measures involving SARS-CoV-2 and the classification as a Risk Group 3 biological agent. *Pathology.* 52, 790-795. https://doi.org/10.1016/j.pathol.2020.09.006

Kiesslich, S., Kamen, A.A. 2020. Vero cell upstream bioprocess development for the production of viral vectors and vaccines. *Biotechnol. Adv.* 44, 107608. https://doi.org/10.1016/j.biotechadv.2020.107608

Kumar, S., Paul, P., Yadav, P., Kaul, R., Maitra, S.S., Jha, S.K., Chaari, A. 2022. A multi-targeted approach to identify potential flavonoids against three targets in the SARS-CoV-2 life cycle. *Comput. Biol. Med.* 142, 105231. https://doi.org/10.1016/j.compbiomed.2022.105231

Lamers, M.M., Haagmans, B.L., 2022. SARS-CoV-2 pathogenesis. *Nat. Rev. Microbiol.* 20, 270-284. https://doi.org/10.1038/s41579-022-00713-0

Liu, J., Li, Y., Liu, Q., Yao, Q., Wang, X., Zhang, H., Chen, R., Ren, L., Min, J., Deng, F., Yan, B. 2021. SARS-CoV-2 cell tropism and multiorgan infection. *Cell Discov.* 7, 1-4. https://doi.org/10.1038/s41421-021-00249-2

Lin, L., Li, Q., Wang, Y. Shi, Y., 2021. Syncytia formation during SARS-CoV-2 lung infection: a disastrous unity to eliminate lymphocytes. *Cell. Death Differ.* 28, 2019-2021. https://doi.org/10.1038/s41418-021-00795-y

Magiorkinis, G., 2022. On the evolution of SARS-CoV-2 and the emergence of Variants of Concern. *Trends Microbiol.* 31, 1-8. https://doi.org/10.1016/j.tim.2022.10.008

Mahajan, S., Caraballo, C., Li, S.X., Dong, Y., Chen, L., Huston, S.K., Srinivasan, R., Redlich, C.A., Ko, A.I., Faust, J.S., Forman, H.P., Krumholz, H.M., 2021. SARS-CoV-2 infection hospitalization rate and infection fatality rate among the non-congregate population in connecticut. *Am. J. Med.* 134, 812-816.e2. https://doi.org/10.1016/j.amjmed.2021.01.020

Murgolo, N., Therien, A.G., Howell, B., Klein, D., Koeplinger, K., Lieberman, L.A., Adam, G.C., Flynn, J., McKenna, P., Swaminathan, G., Hazuda, D.J., Olsen, D.B. 2021. SARS-CoV-2 tropism, entry, replication, and propagation: considerations for drug discovery and development. *PLOS Pathog.* 17, e1009225. https://doi.org/10.1371/journal.ppat.1009225

Narayanan, A., Narwal, M., Majowicz, S,A. Varricchio, C., Toner, S.A., Ballatore, C., Brancale, A., Murakami, K.S., Jose, J. 2022. Identification of SARS-CoV-2 inhibitors targeting Mpro and PLpro using in-cell-protease assay. *Commun. Biol.* 5, 169. https://doi.org/10.1038/s42003-022-03090-9

Noman, A., Aqeel, M., Khalid, N., Hashem, M., Alamari, S., Zafar, S., Qasim, M., Irshad, M.K., Qari, S.H., 2021. Spike glycoproteins: their significance for corona viruses and receptor binding activities for pathogenesis and viral survival. *Microb. Pathog.* 150, 104719. https://doi.org/10.1016/j.micpath.2020.104719

Savastano, A., Ibáñez de Opakua, A., Rankovic, M. Zweckstetter, M., 2020. Nucleocapsid protein of SARS-CoV-2 phase separates into RNA-rich polymerase-containing condensates. *Nat. Commun.* 11, 6041. https://doi.org/10.1038/s41467-020-19843-1

Septisetyani, E.P., Prasetyaningrum, P.W., Anam, K., Santoso, A. 2021. SARS-CoV-2 antibody neutralization assay platforms based on epitopes sources: live virus, pseudovirus, and recombinant S glycoprotein RBD. *Immune Netw.* 21, e39. https://doi.org/10.4110/in.2021.21.e39

Shang, J., Ye, G., Shi, K., Wan, Y., Luo, C., Aihara, H., Geng, Q., Auerbach, A., Li, F., 2020. Structural basis of receptor recognition by SARS-CoV-2. *Nature.* 581, 221–224. https://doi.org/10.1038/s41586-020-2179-y

Sharma, K., Mahato, N., Leem Y.R. 2019. Extraction, characterization and biological activity of citrus flavonoids. *Rev. Chem. Eng.* 35, 265-284. https://doi.org/10.1515/revce-2017-0027

Sun, H., Xu, J., Zhang, G., Han, J., Hao, M., Chen, Z., Fang, T., Chi, X., Yu, C., 2022. Developing pseudovirus-based neutralization assay against omicron-included SARS-CoV-2 variants. *Viruses.* 14, 1332. https://doi.org/10.3390/v14061332

Whitt, M.A. 2010. Generation of VSV pseudotypes using recombinant ΔG-VSV for studies on virus entry, identification of entry inhibitors, and immune responses to vaccines. *J. Virol. Methods.* 169, 365-374. https://doi.org/10.1016/j.jviromet.2010.08.006

Xiao, J., 2017. Dietary flavonoid aglycones and their glycosides: Which show better biological significance? *Crit. Rev. Food Sci. Nutr.* 57, 1874-1905.

Xiao, J., Cao, H., Wang, Y., Zhao, J., Wei, X. 2009. Glycosylation of dietary flavonoids decreases the affinities for plasma protein. *J. Agric. Food Chem.* 57, 6642-6648. https://doi.org/10.1021/jf901456u

Yan, W,. Zheng, Y., Zeng, X. He, B., Cheng, W.. 2022. Structural biology of SARS-CoV-2: open the door for novel therapies. *Sig. Transduct. Target Ther.* 7, 26. https://doi.org/10.1038/s41392-022-00884-5

Yi, L., Ma, S., Ren, D., 2017. Phytochemistry and bioactivity of Citrus flavonoids: a focus on antioxidant, anti-inflammatory, anticancer and cardiovascular protection activities. *Phytochem. Rev.* 16, 479-511. https://doi.org/10.1007/s11101-017-9497-1

Supplementary Materials
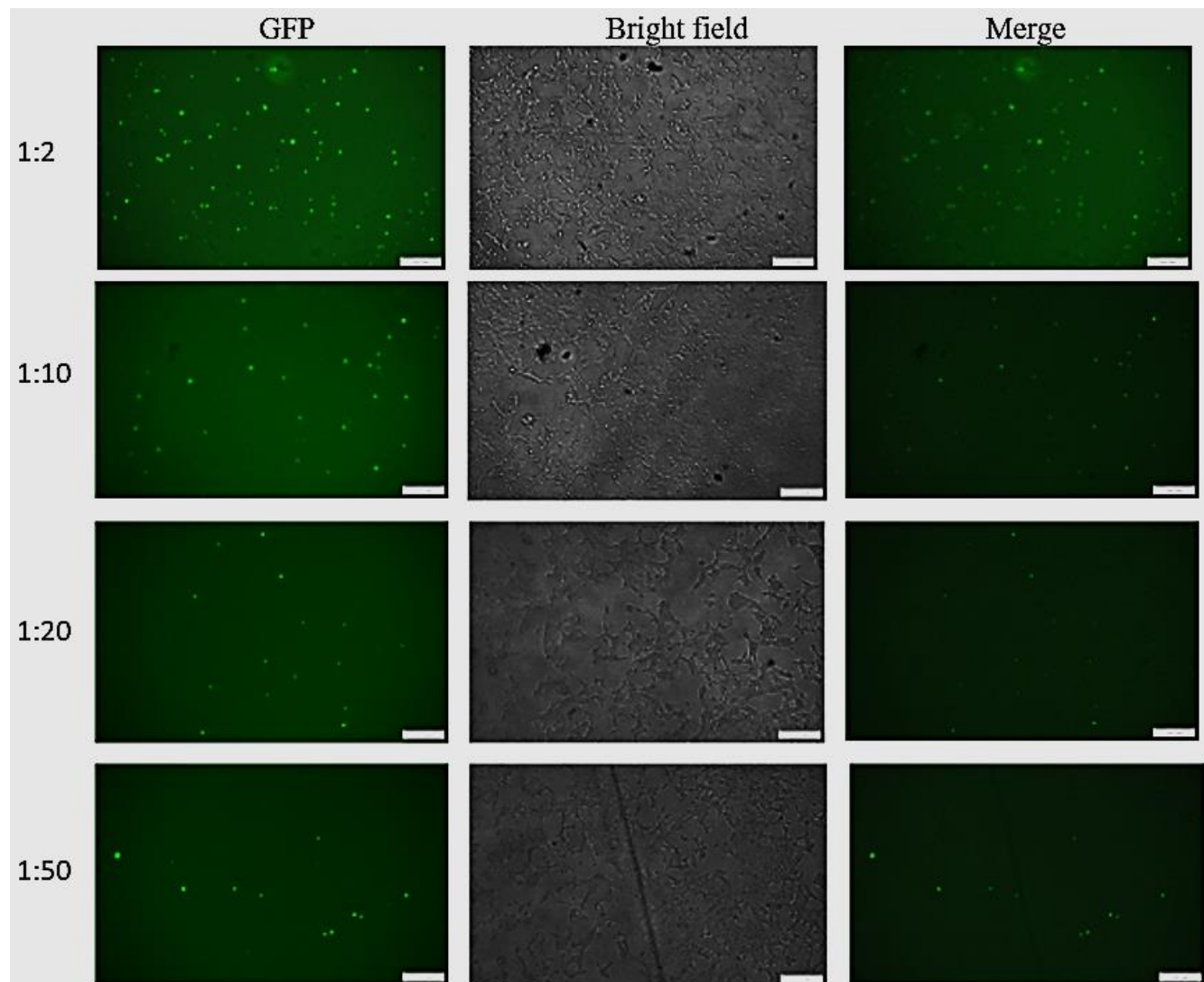
Supplementary Figure 1. Determination of SARS-CoV-2 pseudovirus (rVSV-ΔG/Spike*-GFP) titer in Vero cells
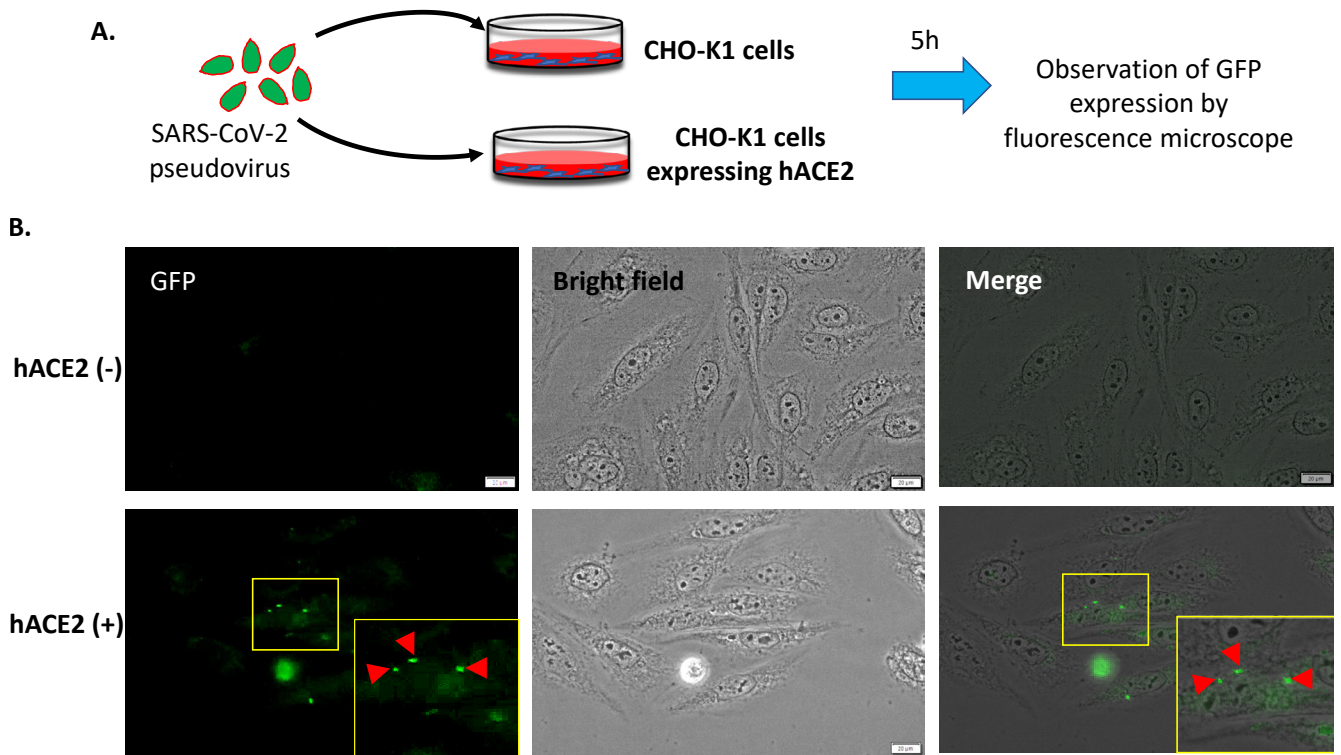
Supplementary Figure 2. Pseudovirus entry assay in CHO-K1 and CHO-K1/hACE2 cells